 CMES, vol.86, no.2, pp.113-144, 2012

Static and Dynamic BEM Analysis of Strain Gradient Elastic Solids and Structures

S.V. Tsinopoulos[1], D. Polyzos[2] and D.E. Beskos[3,4]

Abstract: This paper reviews the theory and the numerical implementation of the direct boundary element method (BEM) as applied to static and dynamic problems of strain gradient elastic solids and structures under two- and three- dimensional conditions. A brief review of the linear strain gradient elastic theory of Mindlin and its simplifications, especially the theory with just one constant (internal length) in addition to the two classical elastic moduli, is provided. The importance of this theory in successfully modeling microstructural effects on the structural response under both static and dynamic conditions is clearly described. The boundary element formulation of static and frequency domain dynamic problems of strain gradient elasticity is accomplished with the aid of reciprocal theorems and corresponding fundamental solutions. Quadratic line and surface boundary elements are developed for two- and three- dimensional problems, respectively. Special crack tip or front, line and surface boundary elements of variable singularity are also developed for fracture mechanics problems. A variety of strain gradient elastic static and dynamic problems involving two- and three- dimensional solids and structures with or without cracks as solved by the BEM are presented in order to illustrate the method, demonstrate its advantages over the finite element method (FEM) and assess and discuss the influence of the microstructure on the response.

Keywords: Boundary elements, Strain gradient elasticity, Microstructural effects, Static analysis, Dynamic analysis, Solids, Structures

[1] Department of Mechanical Engineering, Technological Educational Institute of Patras, GR-26334, Patras, Greece

[2] Department of Mechanical Engineering and Aeronautics, University of Patras, GR-26500 Patras, Greece

[3] Department of Civil Engineering, University of Patras, GR-26500 Patras, Greece

[4] Office of Theoretical and Applied Mechanics, Academy of Athens, 4 Soranou Efessiou str., GR-11527 Athens, Greece

1 Introduction

When linear elastic solids and structures have extremely small dimensions (e.g., microelectronic mechanical systems – MEMS or nanoelectronic mechanical systems – NEMS), which are comparable to their microstructural lengths, their response to static or dynamic loading is significantly influenced by the microstructure of their material. Microstructural effects are also important in problems of localization of deformation, such as stress concentration or crack problems, where the stress field is nonlocal in character. These microstructural effects appear in the form of increased stiffness, size effects, elimination of singularities, increase of natural frequencies and buckling loads and wave dispersion.

Classical linear elasticity cannot take these effects into account and one needs higher order or generalized theories of elasticity with internal length scale parameters, which introduce microstructural effects in a macroscopic manner. Among these theories, one can mention here the general elasticity with microstructure due to Mindlin (1964), the micropolar elasticity due to Eringen (1966), which is similar to that of the Cosserat brothers (1909) and the couple-stress elasticity due to Toupin (1962) and Koiter (1964). A review on these higher-order theories of linear elasticity can be found, e.g., in Tiersten and Bleustein (1974), Vardoulakis and Sulem (1995), Exadaktylos and Vardoulakis (2001) and Askes and Aifantis (2011).

The most general and widely used of all these theories, especially during the last 15 years or so, is the form II version of Mindlin's (1964) theory associated with the second gradient of strain, the gradient elastic theory. This theory, even in its simplified form contains five elastic constants for static problems and seven elastic constants for dynamic problems in addition to the two classical elastic moduli. For reasons of further simplicity, in most applications, usually only one additional constant for static problems and two constants for dynamic problems are retained in the theory.

Among the many existing applications of the above simple strain gradient theory of elasticity with one or two elastic constants for static or dynamic problems, respectively, in addition to the classical ones, one can mention the analytical works of, e.g., Altan and Aifantis (1992), Ru and Aifantis (1993), Vardoulakis et al (1998), Tsepoura et al (2002), Papargyri-Beskou et al (2003), Lazar and Maugin (2005), Giannakopoulos and Stamoulis (2007), Papargyri-Beskou and Beskos (2008, 2009), Georgiadis and Anagnostou (2008), Gao and Ma (2009), Papargyri-Beskou et al (2010) and Aravas (2011) involving static analysis of bars, beams, plates, half-spaces, inclusions, dislocations and cracks and Altan et al (1996), Chang and Gao (1997), Tsepoura et al (2002), Georgiadis et al (2000, 2004), Papargyri-Beskou et al (2003, 2009), Askes and Aifantis (2006), Bennett et al (2007), Papargyri-

Beskou and Beskos (2008), Vavva et al (2009), Papacharalampopoulos et al (2010, 2011) and Polyzos and Fotiadis (2012) involving dynamic analysis of strain gradient beams, plates, bones and lattice models.

Strain gradient elasticity problems with complex geometry and boundary conditions can only be solved by using numerical methods, such as the finite element method (FEM) or the boundary element method (BEM). Apparently, Shu et al (1999) were the first to use the FEM for solving gradient elastic problems under static conditions and they were followed by many others. The main problem with a conventional FEM is the requirement of using elements with $C^{(1)}$ continuity because of the fourth order of the governing equation of equilibrium in terms of displacements. Finite elements with $C^{(1)}$ continuity usually have many degrees of freedom per node involving displacements and displacement gradients. This increases considerably the total number of degrees of freedom and hence the computational effort. However, the method is conceptually simple and easy to implement. One can mention here the works of Akarapu and Zbib (2006), Zervos (2008), Zervos et al (2009), Papanicolopulos et al (2009) and Papanicolopulos and Zervos (2010) and Fischer et al (2010, 2011) dealing mainly with two-dimensional problems. Only the works of Zervos (2008) and Papanicolopulos et al (2009) deal with three-dimensional problems.

The requirement of $C^{(1)}$ continuity can be avoided by various other FEM formulations. The most common such approach is the one employing mixed finite elements in conjunction with Lagrange multipliers or penalty methods. In those FEM's displacements and displacement gradients are treated as independent unknowns possessing $C^{(0)}$ continuity. One can mention here the works of Shu et al (1999), Engel et al (2002), Amanatidou and Aravas (2002), Imatani et al (2005), Giannakopoulos et al (2006), Askes and Gutierrez (2006), Tsamasphyros et al (2007), Markolefas et al (2007, 2008, 2009) and Tsamasphyros and Vrettos (2010) dealing with one- and two-dimensional problems. The FEM of Soh and Chen (2004) and Zhao et al (2011) combines one element with $C^{(0)}$ continuity with another one with $C^{(1)}$ continuity to solve two-dimensional strain gradient elasticity problems. Dessouky et al (2006) combine the standard displacement FEM with the finite difference method to determine the second derivatives of strain in terms of strains at the integration points of the element. Another FEM that avoids $C^{(1)}$ continuity restrictions is the one by Tenek and Aifantis (2002), Askes et al (2008), Gitman et al (2010) and Askes and Aifantis (2011). This method is an operator split method as it decouples the fourth order differential equations of equilibrium into two sets of second order equations each requiring $C^{(0)}$ continuity. Finally, one can mention here the meshless local Petrov-Galerkin method of Tang et al (2003), which by its nature does not have any continuity requirements. Besides this method works with only

displacement degrees of freedom.

The FEM has also been used to solve some one- and two-dimensional strain gradient elastic dynamic problems. One can mention here the works of Bennett et al (2007), Askes et al (2007), Askes et al (2008), Bennett and Askes (2009), Askes and Aifantis (2011) based on the method of operator split and $C^{(0)}$ continuity and of Filopoulos et al (2010) based on one-dimensional elements with $C^{(1)}$ continuity.

A general comment on FEM's used for strain gradient elasticity problems is that, irrespectively of the particular method employed, the number of degrees of freedom is very large and hence the computational cost is very high. Messless methods also require a high computational cost.

The BEM is the ideal numerical method for successfully solving linear elastic static and dynamic problems (Beskos 1987, 1997, 2003). This is because the method i) reduces the dimensionality of the problem by one there by restricting the discretization to the boundary of the body, ii) provides highly accurate results, especially near high stress gradients, iii) does not need absorbing boundaries for infinite or semi-infinite domains and iv) does not require any continuity requirements. The old efficiency problem due to the presence of non-symmetric matrices, has been overcome in recent years with the use of highly efficient equation solvers, such as the fast multipole method (Liu, 2009).

Tsepoura et al (2002) were the first to use the BEM for solving strain gradient elastostatic problems. That work was followed by additional applications of the BEM in gradient elastostatic (Tsepoura and Polyzos 2003, Polyzos et al 2003, Tsepoura et al 2003 and Karlis et al 2007, 2008, 2010) and gradient elastodynamic (Polyzos et al 2003, Tsepoura and Polyzos 2003, Polyzos 2005, Polyzos et al 2005, Karlis et al 2007 and Papacharalampopoulos et al 2010) problems under two- and three-dimensional conditions. At this point one could also mention the recent BEM's of Tsiatas (2009), Tsiatas and Katsikadelis (2011) and Hadjesfandiari and Dargush (2011) for the solution of plate flexure, bar torsion and two-dimensional elastostatic problems involving modified couple stress theories to take into account microstructural effects. The aforementioned basic advantages of the BEM become more pronounced when the method is used for solving strain gradient elastic problems rendering the method a better choice than the FEM.

The present paper reviews all the work that has been done on the development and application of the BEM to strain gradient elastic problems associated with static or dynamic load and two- (2D) and three-dimensional (3D) conditions. The formulation of the method with the aid of the reciprocal theorem and the fundamental solution of the strain gradient elastic problem are first presented. The numerical implementation of the method is presented next. A special crack-tip (front) boundary

element is also presented for fracture mechanics problems. Characteristic numerical examples are presented to illustrate the method and demonstrate its advantages over the FEM. A section of conclusions is finally provided to summarize the results of this work.

2 Strain gradient elastostatic theory

Mindlin (1964), in the Form-II version of his strain gradient elastic theory, considered that the potential energy density W is a quadratic form of the strains ε_{ij} and the gradients of strains, κ_{ijk}, i.e.

$$W = \frac{1}{2}\tilde{\lambda}\varepsilon_{ii}\varepsilon_{jj} + \tilde{\mu}\varepsilon_{ij}\varepsilon_{ij} + \hat{\alpha}_1\kappa_{iik}\kappa_{kjj} + \hat{\alpha}_2\kappa_{ijj}\kappa_{ikk} + \hat{\alpha}_3\kappa_{iik}\kappa_{jjk} + \hat{\alpha}_4\kappa_{ijk}\kappa_{ijk} + \hat{\alpha}_5\kappa_{ijk}\kappa_{kji} \tag{1}$$

where

$$\varepsilon_{ij} = \frac{1}{2}\left(\partial_i u_j + \partial_j u_i\right), \quad \kappa_{ijk} = \partial_i\varepsilon_{jk} = \frac{1}{2}\left(\partial_i\partial_j u_k + \partial_i\partial_k u_j\right) = \kappa_{ikj} \tag{2}$$

with ∂_i denoting space differentiation, u_i being displacements and $\tilde{\lambda}$, $\tilde{\mu}$ and $\hat{\alpha}_1 - \hat{\alpha}_5$ being elastic constants. It should be noted here that for static problems the constants $\tilde{\lambda}$, $\tilde{\mu}$ in Form-II Mindlin's theory are the same with the corresponding Lame constants λ, μ of classical elasticity. Both $\tilde{\lambda}$, $\tilde{\mu}$ have units of N/m^2, whereas $\hat{\alpha}_1 - \hat{\alpha}_5$ have units of force. Thus, this particular case of Mindlin's theory has in total seven elastic constants instead of the 18 constants of his general theory.

Strains ε_{ij} and gradients of strains κ_{ijk} are dual in energy with the Cauchy-like and double stresses, respectively, defined as

$$\tau_{ij} = \frac{\partial W}{\partial \varepsilon_{ij}} = \tau_{ji} \tag{3}$$

$$\mu_{ijk} = \frac{\partial W}{\partial \kappa_{ijk}} = \mu_{ikj} \tag{4}$$

which implies that

$$\tau_{ij} = 2\tilde{\mu}\varepsilon_{ij} + \tilde{\lambda}\varepsilon_{ll}\delta_{ij} \tag{5}$$

and

$$\mu_{ijk} = \frac{1}{2}\hat{\alpha}_1\left[\kappa_{kll}\delta_{ij} + 2\kappa_{lli}\delta_{jk} + \kappa_{jll}\delta_{ki}\right] + 2\hat{\alpha}_2\kappa_{ill}\delta_{jk} + \hat{\alpha}_3\left(\kappa_{llk}\delta_{ij} + \kappa_{llj}\delta_{ik}\right) + 2\hat{\alpha}_4\kappa_{ijk} + \hat{\alpha}_5\left(\kappa_{kij} + \kappa_{jki}\right) \tag{6}$$

The total stress tensor σ_{ij} is then defined as

$$\sigma_{ij} = \tau_{ij} - \partial_i \mu_{ijk}$$

or

$$\sigma = \tau - \nabla \cdot \mu \tag{7}$$

with $-\nabla \cdot \mu$ representing the relative stresses and σ the total stress tensor. Taking the variation of (1) and equilibrating with the work done by external and body forces f_k, one obtains the equilibrium equation

$$\partial_j \left(\tau_{jk} - \partial_i \mu_{ijk} \right) + f_k = 0 \tag{8}$$

accompanied by the classical essential and natural boundary conditions where the displacement vector **u** and/or the traction vector **p** have to be defined on the global boundary S of the analyzed domain, the non-classical essential and natural boundary conditions where the normal displacement vector $\mathbf{q} = \partial \mathbf{u} / \partial \mathrm{n}$ and/or the double traction vector **R** are prescribed on S. The non-classical double traction boundary condition at non-smooth boundaries involves the jump traction vector **E** defined at corners and edges.

Traction vectors **p**, **R**, **E** are defined as

$$p_k = n_j \tau_{jk} - n_i n_j D \mu_{ijk} - \left(n_j D_i + n_i D_j \right) \mu_{ijk} + \left(n_i n_j D_l n_l - D_j n_i \right) \mu_{ijk} \tag{9}$$

$$R_k = n_i n_j \mu_{ijk} \tag{10}$$

$$E_k = \left\| n_i m_j \mu_{ijk} \right\| \tag{11}$$

where **n** is the unit vector normal to the global boundary S, $D = n_l \partial_l$ and $D_j = \left(\delta_{jl} - n_j n_l \right) \partial_l$. The non-classical boundary condition (11) exists only when non-smooth boundaries are considered. Double brackets $\|\bullet\|$ indicate that the enclosed quantity is the difference between its values taken on the two sides of a corner, whereas **m** is a vector being tangential to the corner line.

Finally, taking into account the form of τ and μ, the equilibrium equation (8) in terms of displacements is written as

$$\left(\tilde{\lambda} + 2\tilde{\mu} \right) \left(1 - \mathrm{l}_1^2 \nabla^2 \right) \nabla \nabla \cdot \mathbf{u} + \tilde{\mu} \left(1 - \mathrm{l}_2^2 \nabla^2 \right) \nabla \times \nabla \times \mathbf{u} + \mathbf{f} = \mathbf{0} \tag{12}$$

where

$$l_1^2 = 2 \left(\hat{\alpha}_1 + \hat{\alpha}_2 + \hat{\alpha}_3 + \hat{\alpha}_4 + \hat{\alpha}_5 \right) / \left(\tilde{\lambda} + 2\tilde{\mu} \right) \tag{13}$$

$$l_2^2 = (\hat{\alpha}_3 + 2\hat{\alpha}_4 + \hat{\alpha}_5)/2\tilde{\mu} \tag{14}$$

l_1^2 and l_2^2 have units of m^2 and as it is discussed in Ben Amoz (1976) and Vavva et al (2009), both can be considered as internal length-scale parameters, which correlate the microstructure with the macrostructure in irrotational and solenoidal deformations, respectively.

For the particular case of $\hat{\alpha}_1 = \hat{\alpha}_3 = \hat{\alpha}_5 = 0,\ \hat{\alpha}_2 = (1/2)\lambda g^2, \hat{\alpha}_4 = \mu g^2,\ \tilde{\lambda} = \lambda$ and $\tilde{\mu} = \mu$ one obtains the simple strain gradient elasticity theory with just one constant, g, with dimensions of length in addition to the two classical elastic moduli λ and μ (Lamé constants). In this case one has from Eqs (13) and (14) that l_1^2=l_2^2=g^2, while Eq. (12) takes the form

$$\left(1-g^2\nabla^2\right)\left[\mu\nabla^2\mathbf{u}+(\lambda+\mu)\nabla\nabla\cdot\mathbf{u}\right]+\mathbf{f}=0 \tag{15}$$

The only nonclassical constant g is called volumetric gradient elastic constant or simply gradient coefficient.

3 Fundamental solution and integral representation

For an infinitely extended gradient elastic space, the fundamental solution of Eq. (12) is represented by a second-order tensor $\mathbf{U}^*(\mathbf{x},\mathbf{y})$ satisfying the partial differential equation

$$\left(\tilde{\lambda}+2\tilde{\mu}\right)\left(1-l_1^2\nabla^2\right)\nabla\nabla\cdot\mathbf{U}^*(\mathbf{x},\mathbf{y})-\mu\left(1-l_2^2\nabla^2\right)\nabla\times\nabla\times\mathbf{U}^*(\mathbf{x},\mathbf{y})=-\delta(\mathbf{x},\mathbf{y})\widetilde{\mathbf{I}} \tag{16}$$

where δ is the Dirac delta function and $\mathbf{x}$ is the point (field point) where the displacement $\mathbf{U}^*(\mathbf{x},\mathbf{y})$ is obtained due to a unit force at point $\mathbf{y}$ (source point).

It can be proved (Karlis et al 2010) that the solution of Eq. (16) has the form

$$U_{ij}^*=\frac{1}{16\pi\mu(1-\nu)}\left[\Psi(r)\,\delta_{ij}-X(r)\hat{r}_i\hat{r}_j\right] \tag{17}$$

where $\nu=\tilde{\lambda}/\left(2\left(\tilde{\lambda}+\tilde{\mu}\right)\right)$ is the Poisson ratio, $r=|\mathbf{x}-\mathbf{y}|$, $\hat{\mathbf{r}}=(\mathbf{x}-\mathbf{y})/(|\mathbf{x}-\mathbf{y}|)$ and

$$\begin{aligned} X(r) = &-\tfrac{1}{r}+2(1-2\nu)\left[\left(\tfrac{3l_1^2}{r^3}+\tfrac{3l_1}{r^2}+\tfrac{1}{r}\right)e^{-r/l_1}-\tfrac{3l_1^2}{r^3}\right] \\ &-4(1-\nu)\left[\left(\tfrac{3l_2^2}{r^3}+\tfrac{3l_2}{r^2}+\tfrac{1}{r}\right)e^{-r/l_2}-\tfrac{3l_2^2}{r^3}\right] \end{aligned} \tag{18}$$

$$\begin{aligned} \Psi(r) = &(3-4\nu)\tfrac{1}{r}+2(1-2\nu)\left[\left(\tfrac{l_1^2}{r^3}+\tfrac{l_1}{r^2}\right)e^{-r/l_1}-\tfrac{l_1^2}{r^3}\right] \\ &-4(1-\nu)\left[\left(\tfrac{l_2^2}{r^3}+\tfrac{l_2}{r^2}+\tfrac{1}{r}\right)e^{-r/l_2}-\tfrac{l_2^2}{r^3}\right] \end{aligned} \tag{19}$$

for three dimensions and

$$\mathrm{X}(r) = -1 + 2(1-2\nu)\left[K_2\left(\frac{r}{l_1}\right) - \frac{2l_1^2}{r^2}\right] - 4(1-\nu)\left[K_2\left(\frac{r}{l_2}\right) - \frac{2l_2^2}{r^2}\right] \tag{20}$$

$$\begin{aligned}\Psi(r) = &-(3-4\nu)\ln(r) + 2(1-2\nu)\left[\frac{l_1}{r}K_1\left(\frac{r}{l_1}\right) - \frac{l_1^2}{r^2}\right] \\ &-4(1-\nu)\left[K_0\left(\frac{r}{l_2}\right) + \frac{l_2}{r}K_1\left(\frac{r}{l_2}\right) - \frac{l_2^2}{r^2}\right]\end{aligned} \tag{21}$$

for two dimensions, with $\mathrm{K_n(r/l_i)}$ being the modified Bessel functions of the second kind and nth order.

Utilizing the expansions of $\mathrm{e^{-r/l_i}}$ and $\mathrm{K_n(r/l_i)}$, it is easy to prove that both functions X, Ψ given by relations (18) – (21) are regular as $\mathrm{r} \to 0$ according to the asymptotic relations

$$\mathrm{X(r) = O\left(r^2 lnr\right)}, \quad \Psi(\mathrm{r}) = \mathrm{O}(1) \text{ for the 2D case}$$

$$\mathrm{X(r) = O(r)}, \quad \Psi(\mathrm{r}) = \mathrm{O}(1) \text{ for the 3D case} \tag{22}$$

Consider the two elastostatic states **u, P, R, E** and **u*, P*, R*, E*** of a gradient elastic finite body with volume V and surface S. For this body the following reciprocity identity holds true (Polyzos et al 2003, Karlis et al 2010) :

$$\begin{aligned}&\int_V \{\mathbf{f}^* \cdot \mathbf{u} - \mathbf{f} \cdot \mathbf{u}^*\}\, \mathrm{d}V + \int_S \{\mathbf{P}^* \cdot \mathbf{u} - \mathbf{P} \cdot \mathbf{u}^*\}\, \mathrm{d}S = \int_S \left\{\mathbf{R} \cdot \frac{\partial \mathbf{u}^*}{\partial n} - \mathbf{R}^* \cdot \frac{\partial \mathbf{u}}{\partial n}\right\} \mathrm{d}S + \\ &\sum_{C_a} \oint_{C_a} \{\mathbf{E} \cdot \mathbf{u}^* - \mathbf{E}^* \cdot \mathbf{u}\}\, \mathrm{d}C\end{aligned} \tag{23}$$

In the above, **f** represent body forces and **P, R, E** are traction, double traction and jump traction vectors, respectively, defined in (9) – (11), while C_a represents the edge lines formed by the intersection of two surface portions when the boundary S is non-smooth. For a plane non-smooth boundary, where parts of the global boundary form C_a corners one has again Eq. (23) but with the last term in its right hand side replaced by $\sum_{C_a} \{\mathbf{E} \cdot \mathbf{u}^* - \mathbf{E}^* \cdot \mathbf{u}\}$.

Assume that the displacement field $\mathbf{u}^*$, appearing in the reciprocity identity (23), is the result of a body force having the form

$$\mathbf{f}^*(\mathbf{y}) = \delta(\mathbf{x} - \mathbf{y})\,\widehat{\mathbf{e}} \tag{24}$$

with $\widehat{\mathbf{e}}$ being the direction of a unit force acting at point **y**. Recalling the definition of the fundamental solution, it is easy to see that the displacement field **u*** due to **f*** can be represented by means of the fundamental displacement tensor $\mathbf{U}^*(\mathbf{x}, \mathbf{y})$ given by Eqs (17) and (18) – (21), according to the relation

$$\mathbf{u}^*(\mathbf{y}) = \mathbf{U}^*(\mathbf{x}, \mathbf{y}) \cdot \widehat{\mathbf{e}} \tag{25}$$

Inserting the above expression of **U*** in (23) and assuming zero body forces **f**=0, one obtains the boundary integral equation

$$\tilde{\mathbf{c}}(\mathbf{x})\cdot\mathbf{u}(\mathbf{x})+\int_S\{\mathbf{P}^*(\mathbf{x},\mathbf{y})\cdot\mathbf{u}(\mathbf{y})-\mathbf{U}^*(\mathbf{x},\mathbf{y})\cdot\mathbf{P}(\mathbf{y})\}\,\mathrm{d}S_{\mathbf{y}}=$$
$$\int_S\{\mathbf{Q}^*(\mathbf{x},\mathbf{y})\cdot\mathbf{R}(\mathbf{y})-\mathbf{R}^*(\mathbf{x},\mathbf{y})\cdot\mathbf{q}(\mathbf{y})\}\,\mathrm{d}S_{\mathbf{y}}+$$
$$\sum_{C_a}\oint_{\mathbf{C}}\{\mathbf{U}^*(\mathbf{x},\mathbf{y})\cdot\mathbf{E}(\mathbf{y})-\mathbf{E}^*(\mathbf{x},\mathbf{y})\cdot\mathbf{u}(\mathbf{y})\}\,\mathrm{d}C_y \quad (26)$$

where $\tilde{\mathbf{c}}(\mathbf{x})$ is the well-known jump-tensor of classical boundary integral representations (Polyzos et al 2003) and the symbols $\mathbf{Q}^*,\mathbf{q}$ have been used instead of $\partial\mathbf{U}^*/\partial n$, $\partial\mathbf{u}/\partial n$, respectively.

Of course, for plane problems there is no integral sign in the last right hand side term of Eq. (26) and C_a refers to corners.

In case the boundary S is smooth and the point **x** belongs to S, then the integral equation (26) reduces to

$$\frac{1}{2}\mathbf{u}(\mathbf{x})+\int_S\{\mathbf{P}^*(\mathbf{x},\mathbf{y})\cdot\mathbf{u}(\mathbf{y})-\mathbf{U}^*(\mathbf{x},\mathbf{y})\cdot\mathbf{P}(\mathbf{y})\}\,\mathrm{d}S_y=$$
$$\int_S\{\mathbf{Q}^*(\mathbf{x},\mathbf{y})\cdot\mathbf{R}(\mathbf{y})-\mathbf{R}^*(\mathbf{x},\mathbf{y})\cdot\mathbf{q}(\mathbf{y})\}\,\mathrm{d}S_y \quad (27)$$

Observing Eq. (27), one easily realizes that it contains four unknown vector fields, $\mathbf{u}(\mathbf{x})$, $\mathbf{P}(\mathbf{x})$, $\mathbf{R}(\mathbf{x})$ and $\mathbf{q}(\mathbf{x})$ while the boundary conditions are two (classical and non-classical). Thus, the evaluation of the unknown fields requires the existence of one more integral equation. This integral equation is obtained by applying the operator $\partial/\partial n_x$ on (27) and has the form

$$\frac{1}{2}\mathbf{q}(\mathbf{x})+\int_S\left\{\frac{\partial\mathbf{P}^*(\mathbf{x},\mathbf{y})}{\partial n_x}\cdot\mathbf{u}(\mathbf{y})-\frac{\partial\mathbf{U}^*(\mathbf{x},\mathbf{y})}{\partial n_x}\cdot\mathbf{P}(\mathbf{y})\right\}\mathrm{d}S_y=$$
$$\int_S\left\{\frac{\partial\mathbf{Q}^*(\mathbf{x},\mathbf{y})}{\partial n_x}\cdot\mathbf{R}(\mathbf{y})-\frac{\partial\mathbf{R}^*(\mathbf{x},\mathbf{y})}{\partial n_x}\cdot\mathbf{q}(\mathbf{y})\right\}\mathrm{d}S_y \quad (28)$$

The pair of integral equations (27) and (28) accompanied by the classical and non-classical boundary conditions form the integral representation of any Mindlin's Form-II strain gradient elastic boundary value problem with 3D or 2D smooth boundary. Full expressions of the integral equations for non-smooth boundaries can be found in Karlis et al (2010).

4 BEM formulation

The goal of the BEM is to solve numerically the boundary integral representation of the problem presented in the previous section. To this end, the boundary S is discretized into E quadratic continuous isoparametric elements each of which has $A(e)$ nodes, with $A(e)$= 3, 8, 6 when line, quadrilateral and triangular elements, respectively, are considered. For the boundary of the domain B, three noded line quadratic elements have been taken into account. For a nodal point k, the discretized integral equations (27) and (28) for the 3D case have the form

$$\begin{aligned}
&\frac{1}{2}u\left(x^k\right)+\sum_{e=1}^{E}\sum_{a=1}^{A(e)}\int_{-1}^{1}\int_{-1}^{1}P^*\left(x^k,y^e\left(\xi_1,\xi_2\right)\right)N^a\left(\xi_1,\xi_2\right)J\left(\xi_1,\xi_2\right)d\xi_1 d\xi_2\cdot u_a^e\\
&+\sum_{e=1}^{E}\sum_{a=1}^{A(e)}\int_{-1}^{1}\int_{-1}^{1}R^*\left(x^k,y^e\left(\xi_1,\xi_2\right)\right)N^a\left(\xi_1,\xi_2\right)J\left(\xi_1,\xi_2\right)d\xi_1 d\xi_2\cdot q_a^e\\
&=\sum_{e=1}^{E}\sum_{a=1}^{A(e)}\int_{-1}^{1}\int_{-1}^{1}U^*\left(x^k,y^e\left(\xi_1,\xi_2\right)\right)N^a\left(\xi_1,\xi_2\right)J\left(\xi_1,\xi_2\right)d\xi_1 d\xi_2\cdot P_a^e\\
&\qquad+\sum_{e=1}^{E}\sum_{a=1}^{A(e)}\int_{-1}^{1}\int_{-1}^{1}Q^*\left(x^k,y^e\left(\xi_1,\xi_2\right)\right)N^a\left(\xi_1,\xi_2\right)J\left(\xi_1,\xi_2\right)d\xi_1 d\xi_2\cdot R_a^e \quad (29)
\end{aligned}$$

$$\begin{aligned}
&\frac{1}{2}q\left(x^k\right)+\sum_{e=1}^{E}\sum_{a=1}^{A(e)}\int_{-1}^{1}\int_{-1}^{1}\frac{\partial}{\partial n_x}P^*\left(x^k,y^e\left(\xi_1,\xi_2\right)\right)N^a\left(\xi_1,\xi_2\right)J\left(\xi_1,\xi_2\right)d\xi_1 d\xi_2\cdot u_a^e\\
&+\sum_{e=1}^{E}\sum_{a=1}^{A(e)}\int_{-1}^{1}\int_{-1}^{1}\frac{\partial}{\partial n_x}R^*\left(x^k,y^e\left(\xi_1,\xi_2\right)\right)N^a\left(\xi_1,\xi_2\right)J\left(\xi_1,\xi_2\right)d\xi_1 d\xi_2\cdot q_a^e\\
&=\sum_{e=1}^{E}\sum_{a=1}^{A(e)}\int_{-1}^{1}\int_{-1}^{1}\frac{\partial}{\partial n_x}U^*\left(x^k,y^e\left(\xi_1,\xi_2\right)\right)N^a\left(\xi_1,\xi_2\right)J\left(\xi_1,\xi_2\right)d\xi_1 d\xi_2\cdot P_a^e\\
&\qquad+\sum_{e=1}^{E}\sum_{a=1}^{A(e)}\int_{-1}^{1}\int_{-1}^{1}\frac{\partial}{\partial n_x}Q^*\left(x^k,y^e\left(\xi_1,\xi_2\right)\right)N^a\left(\xi_1,\xi_2\right)J\left(\xi_1,\xi_2\right)d\xi_1 d\xi_2\cdot R_a^e \quad (30)
\end{aligned}$$

with N^a representing shape functions, the first summation is over the elements, the second summation over the element nodes and J is the Jacobian of the transformation from the global coordinate system to the local coordinate system of the element. Finally, u_a^e, q_a^e, P_a^e and R_a^e are the values of the unknown fields at the nodes of element e.

When the source point does not coincide with the field point, all the above integrals are non-singular and can be easily computed by Gauss quadrature. In case these

two points coincide, the integrals become singular and are computed by the special method of Guiggiani (1998), as described in detail in Tsepoura et al (2003).

Collocating the boundary integral equations (29) and (30) at nodal boundary points, one can obtain a linear system of equations of the form

$$\begin{bmatrix} \frac{1}{2}\widetilde{\mathbf{I}}+\widetilde{\mathbf{H}} & \widetilde{\mathbf{K}} \\ \widetilde{\mathbf{S}} & \frac{1}{2}\widetilde{\mathbf{I}}+\widetilde{\mathbf{T}} \end{bmatrix} \cdot \begin{bmatrix} \mathbf{u} \\ \mathbf{q} \end{bmatrix} = \begin{bmatrix} \widetilde{\mathbf{G}} & \widetilde{\mathbf{L}} \\ \widetilde{\mathbf{V}} & \widetilde{\mathbf{W}} \end{bmatrix} \cdot \begin{bmatrix} \mathbf{P} \\ \mathbf{R} \end{bmatrix} \tag{31}$$

where the various matrices $\widetilde{\mathbf{H}}$, $\widetilde{\mathbf{K}}$, $\widetilde{\mathbf{S}}$, etc. contain elements which are integrals with integrands the various kernels coming from the fundamental solution.

This system after application of the classical and the non-classical boundary conditions and rearrangement results into a linear system of equations of the form $\mathbf{A}\cdot\mathbf{x}=\mathbf{b}$, where $\mathbf{A}$ is a non-symmetric and fully populated matrix, whereas the vectors $\mathbf{x}$ and $\mathbf{b}$ contain all the unknown and known nodal components of the boundary fields, respectively. Finally, the above linear system is solved via a typical LU-decomposition algorithm and the vector $\mathbf{x}$, comprising all the unknown nodal values of **u, q, R** and **P**, is evaluated. As soon as the boundary parameters are known, the internal displacement field is easily evaluated with the aid of (26) with $\widetilde{\mathbf{c}}(\mathbf{x}) = 1$.

5 Special crack tip (front) boundary elements

According to Exadaktylos et al (1996), Vardoulakis and Exadaktylos (1997), Exadaktylos (1998), Zhang et al (1998), Fannjiang et al (2002), Georgiadis (2003), Aravas and Giannakopoulos (2009) and Gourgiotis and Georgiadis (2009), who have studied analytically the asymptotic behavior of displacements and stresses around the tip of a crack under plane conditions, the fields **u, q, R** and **P** near the crack tip vary as $r^{3/2}$, $r^{1/2}$, $r^{-1/2}$ and $r^{-3/2}$, respectively, with r being the distance from the crack tip. As it is well known, the elements used in a classical BEM formulation interpolate the unknown fields either linearly or quadratically and therefore the behavior of the fields around the crack tip can never be represented correctly. Adoption of the idea of Lim et al (2002) of using variable-order singularity boundary elements around the tip of the crack for the description of the near tip behavior and the evaluation of the corresponding stress intensity factors (SIFs), can lead to a new special variable order of singularity discontinuous element. The advantage of this approach is that the fields around the tip of the crack are treated in a unified manner.

In this special element, the functional nodes are identical to those of a classical discontinuous three-noded quadratic line element, with the geometrical node residing always at the crack tip. The main advantage of using discontinuous elements

is that no functional nodes are located at the tip of the crack and thus, despite the singularity of **R** and **P** at the tip, their nodal values are finite and can be computed.

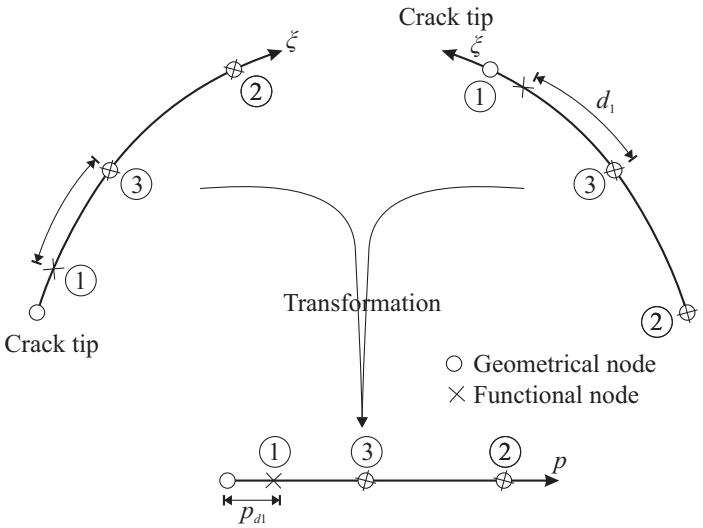

Figure 1: Variable-order singularity discontinuous boundary element and its transformation.

As shown in Fig. 1, the tip of the crack can be located either at $\xi = -1$ or at $\xi = 1$ for the special element being to the left or right of the tip. In order to unify these two possible cases, a new variable p is introduced via the linear transformation

$$p = (1 + c\xi)/2 \tag{32}$$

with $c = \pm 1$ for the tip located at $\xi \mp 1$, respectively,. Thus, the tip of the crack is always located at $p = 0$ and the interval $\xi \in [-1,\ 1]$ is transformed into the interval $p \in [0,\ 1]$. The fields, in terms of the asymptotic solutions, can be expressed as

$$\mathbf{F} = \mathbf{K}_1 \mathrm{r}^{\lambda_1} + \mathbf{K}_2 \mathrm{r}^{\lambda_2} + \mathbf{C} \tag{33}$$

where $\mathbf{K}_1$, $\mathbf{K}_2$ and $\mathbf{C}$ are constant vectors to be determined, the symbol $\mathbf{F}$ represents **u, q, R** or **P** and λ_1 and λ_2 take the values of Table 1.

Writing Eq. (33) for the three functional nodes of the variable-order of singularity discontinuous element one obtains the linear system of equations

$$\begin{aligned} r = p_{d_1} L:&\ \mathbf{K}_1 \left(L p_{d_1}\right)^{\lambda_1} + \mathbf{K}_2 \left(L p_{d_1}\right)^{\lambda_2} + \mathbf{C} = \mathbf{F}_1 \\ r = \tfrac{L}{2}:&\ \mathbf{K}_1 \left(\tfrac{L}{2}\right)^{\lambda_1} + \mathbf{K}_2 \left(\tfrac{L}{2}\right)^{\lambda_2} + \mathbf{C} = \mathbf{F}_3 \\ r = L:&\ \mathbf{K}_1 L^{\lambda_1} + \mathbf{K}_2 L^{\lambda_2} + \mathbf{C} = \mathbf{F}_2 \end{aligned} \tag{34}$$

where $\mathbf{F}_1$, $\mathbf{F}_2$ and $\mathbf{F}_3$ are the nodal values of field $\mathbf{F}$, p_{d_1} is the local coordinate of the discontinuous functional node and L is the length of the element. In the present work p_{d_1} is considered to be equal to 1/6. The solution of the linear system (34) yields the parameters $\mathbf{K}_1$, $\mathbf{K}_2$ and $\mathbf{C}$ as functions of the nodal values $\mathbf{F}_1$, $\mathbf{F}_2$ and $\mathbf{F}_3$. Substituting $\mathbf{K}_1$, $\mathbf{K}_2$ and $\mathbf{C}$ into Eq. (33), rearranging with respect to the nodal values $\mathbf{F}_1$, $\mathbf{F}_2$ and $\mathbf{F}_3$ and taking into account that the distance from the tip of the crack is $r = Lp$, the field $\mathbf{F}$ can be written as

$$\mathbf{F} = N_1\mathbf{F}_1 + N_2\mathbf{F}_2 + N_3\mathbf{F}_3 \tag{35}$$

where the interpolation functions $\mathrm{N}_i = \mathrm{N}_i(p, \lambda_1, \lambda_2)$ can be found explicitly in Karlis et al (2007). These interpolation functions for the fields $\mathbf{R}$ and $\mathbf{P}$ become singular when approaching the tip of the crack $(p \to 0)$.

Table 1: Orders of magnitude of the asymptotic fields

F	λ_1	λ_2
u	3/2	1
q	1/2	1
R	-1/2	1
P	-3/2	-1/2

In Eqs. (29) and (30), the integrals involving the fields $\mathbf{P}$ and $\mathbf{R}$ and defined over the special boundary elements, in addition to the usual fundamental solution type of singularities, exhibit an extra singularity due to the singular behavior of the interpolation functions near the tip of the crack. Thus, even in cases where the source point does not reside in the element, i.e. in cases where a so-called regular integration is performed, there is always present a singularity near the tip of the crack.

The methodology for the treatment of these integrals deals first with the handling of the singularities coming from the interpolation functions of the special element and then addresses any possible singularities that are introduced by the fundamental solutions (in case the source point resides in the element). For more details one should consult Karlis et al (2007).

Once the boundary value problem has been solved, the calculation of SIFs is done via the three nodal traction values of the special elements.

Approaching the crack tip $(r \to 0)$, the traction $\mathbf{P}$, according to Eq. (33), admits a representation of the form

$$\mathbf{P} = \frac{\mathbf{K}_1(\mathbf{P}_1, \mathbf{P}_2, \mathbf{P}_3)}{\sqrt{2\pi}} \lim_{r\to 0} r^{-3/2} + \frac{\mathbf{K}_2(\mathbf{P}_1, \mathbf{P}_2, \mathbf{P}_3)}{\sqrt{2\pi}} \lim_{r\to 0} r^{-1/2} \tag{36}$$

where the components of the vectors $\mathbf{K}_1$ and $\mathbf{K}_2$, obtained by solving the system (34), stand for the stress intensity factors corresponding to x and y directions, respectively, according to the relations

$$\mathbf{K}_1 = \left\{ \begin{array}{c} K_{1x} \\ K_{1y} \end{array} \right\} = L^{3/2}\sqrt{2\pi}\, p_{d_1} \frac{\sqrt{p_{d_1}}\left(2-\sqrt{2}\right)\mathbf{P}_1+\left(\sqrt{2}-2\sqrt{p_{d_1}}\right)\mathbf{P}_2-\left(\sqrt{2}-\sqrt{2p_{d_1}}\right)\mathbf{P}_3}{2-\sqrt{2}+\left(-4+\sqrt{2}\right)p_{d_1}+2p_{d_1}^{3/2}}$$

$$\mathbf{K}_2 = \left\{ \begin{array}{c} K_{2x} \\ K_{2y} \end{array} \right\} = \sqrt{L}\sqrt{2\pi} \frac{p_{d_1}^{3/2}\left(\sqrt{2}-4\right)\mathbf{P}_1+\left(4p_{d_1}^{3/2}-\sqrt{2}\right)\mathbf{P}_2+\sqrt{2}\left(1-p_{d_1}^{3/2}\right)\mathbf{P}_3}{2-\sqrt{2}+\left(-4+\sqrt{2}\right)p_{d_1}+2p_{d_1}^{3/2}} \tag{37}$$

where $\mathbf{P}_1$, $\mathbf{P}_2$ and $\mathbf{P}_3$are the nodal values of **P.**

Near the crack front of a three-dimensional crack problem, the fields **u, q, R** and **P** vary with the distance r from that front in the same way as in the plane case. For this case special discontinuous quadrilateral, eight-noded boundary elements with variable order singularity are constructed for the treatment of the fields around the crack front by following the idea of Zhou et al (2005). More details about these elements and their implementation in the BEM for solving three-dimensional crack problems can be found in Karlis et al (2008).

6 Strain gradient elastodynamics by BEM

Consider the case of strain gradient elastodynamics, which is governed by the equation of motion (Papacharalampopoulos et al 2010)

$$(\tilde{\lambda}+2\tilde{\mu})(1-l_1^2\nabla^2)\nabla\nabla\cdot\mathbf{u}+\tilde{\mu}(1-l_2^2\nabla^2)\nabla\times\nabla\times\mathbf{u}+f = \rho\left(\ddot{\mathbf{u}}-h_1^2\nabla\nabla\cdot\ddot{\mathbf{u}}+h_2^2\nabla\times\nabla\times\ddot{\mathbf{u}}\right) \tag{38}$$

where h_1^2, h_2^2 are intrinsic microinertia coefficients, explicitly defined in Mindlin (1964), while overdots denote time differentiation. Assuming for all the fields involved a harmonic time dependence, e.g.,$u(x,t) = \bar{u}(x)e^{i\omega t}$, where ω is the frequency and t the time, Eq. (38) takes the form

$$(\lambda+2\mu)\left(1-l_1^2\Delta\right)\nabla\nabla\cdot\bar{\mathbf{u}}-\mu\left(1-l_2^2\Delta\right)\nabla\times\nabla\times\bar{\mathbf{u}} +\rho\omega^2\left(\bar{\mathbf{u}}-h_1^2\nabla\nabla\cdot\bar{\mathbf{u}}+h_2^2\nabla\times\nabla\times\bar{\mathbf{u}}\right)+\bar{f}=0 \tag{39}$$

The fundamental solution $\mathbf{U}^*(\mathrm{r})$ of Eq. (39) is defined for the case of $\bar{\mathbf{f}}=\delta(\mathbf{x}-\mathbf{y})\mathbf{I}$ and for the 3D case has the form (Papacharalampopoulos et al 2010)

$$\mathbf{U}^*(\mathbf{x},\mathbf{y}) = \frac{1}{2^{\alpha-1}\pi\rho\omega^2}\left[\Psi(r)\tilde{\mathbf{I}}-\mathrm{X}(r)\left(\hat{\mathbf{r}}\otimes\hat{\mathbf{r}}\right)\right] \tag{40}$$

where $\mathrm{r}=|\mathrm{x}-\mathrm{y}|$, $\widehat{\mathbf{r}}=(\mathbf{x}-\mathbf{y})/(|\mathbf{x}-\mathbf{y}|)$, α is the dimensions number (2 or 3) and X and Ψ are scalar functions given by the relations

$$\begin{aligned}
\mathrm{X}(r) &= \frac{1+L_1^2k_1^2}{1+2L_1^2k_1^2}(k_1^2-\frac{3ik_1}{r}-\frac{3}{r^2})\frac{e^{-ik_1r}}{r}-\frac{1+L_2^2k_2^2}{1+2L_2^2k_2^2}(k_2^2-\frac{3ik_2}{r}-\frac{3}{r^2})\frac{e^{-ik_2r}}{r}\\
&-\frac{L_1^2k_1^2}{1+2L_1^2k_1^2}(a_1^2+\frac{3a_1}{r}+\frac{3}{r^2})\frac{e^{-a_1r}}{r}+\frac{L_2^2k_2^2}{1+2L_2^2k_2^2}(a_2^2+\frac{3a_2}{r}+\frac{3}{r^2})\frac{e^{-a_2r}}{r}\\
\Psi(r) &= \frac{1+L_1^2k_1^2}{1+2L_1^2k_1^2}(\frac{ik_1}{r}+\frac{1}{r^2})\frac{e^{-ik_1r}}{r}-\frac{1+L_2^2k_2^2}{1+2L_2^2k_2^2}(-k_2^2+\frac{ik_2}{r}+\frac{1}{r^2})\frac{e^{-ik_2r}}{r}\\
&-\frac{L_1^2k_1^2}{1+2L_1^2k_1^2}(\frac{a_1}{r}+\frac{1}{r^2})\frac{e^{-a_1r}}{r}-\frac{L_2^2k_2^2}{1+2L_2^2k_2^2}(a_2^2+\frac{a_2}{r}+\frac{1}{r^2})\frac{e^{-a_2r}}{r}
\end{aligned} \tag{41}$$

for 3D and

$$\begin{aligned}
\mathrm{X}(r) &= \frac{1+L_1^2k_1^2}{1+2L_1^2k_1^2}k_1^2K_2(ik_1r)-\frac{1+L_2^2k_2^2}{1+2L_2^2k_2^2}k_2^2K_2(ik_2r)\\
&-\frac{1+L_1^2k_1^2}{1+2L_1^2k_1^2}k_1^2K_2(a_1r)+\frac{1+L_2^2k_2^2}{1+2L_2^2k_2^2}k_2^2K_2(a_1r)\\
\Psi(r) &= -\frac{1+L_1^2k_1^2}{1+2L_1^2k_1^2}\frac{k_1^2}{2}[K_2(ik_1r)-K_0(ik_1r)]\\
&+\frac{1+L_2^2k_2^2}{1+2L_2^2k_2^2}\frac{k_2^2}{2}[K_2(ik_2r)+K_0(ik_2r)]\\
&-\frac{1+L_1^2k_1^2}{1+2L_1^2k_1^2}\frac{k_1^2}{2}[K_0(a_1r)-K_2(a_1r)]\\
&+\frac{1+L_2^2k_2^2}{1+2L_2^2k_2^2}\frac{k_2^2}{2}[K_0(a_2r)+K_2(a_2r)]
\end{aligned} \tag{42}$$

for 2D , where

$$\begin{aligned}
&k_1^2\left(1+L_1^2k_1^2\right)=k_P^2,\ \mathrm{k}_2^2\left(1+L_2^2k_2^2\right)=k_S^2\\
&k_P=\sqrt{\frac{\rho\omega^2}{\lambda+2\mu-\rho\omega^2h_1^2}},\ \mathrm{k}_S=\sqrt{\frac{\rho\omega^2}{\mu-\rho\omega^2h_2^2}}\\
&L_1=l_1\sqrt{\frac{\lambda+2\mu}{\lambda+2\mu-\rho\omega^2h_1^2}},\ L_2=l_2\sqrt{\frac{\mu}{\mu-\rho\omega^2h_2^2}}\\
&a_1=\sqrt{\frac{1}{L_1^2}+k_1^2},\ a_2=\sqrt{\frac{1}{L_2^2}+k_2^2}
\end{aligned} \tag{43}$$

Following exactly the same procedure as in the elastostatic case, one can finally obtain the boundary integral representation of the frequency domain elastodynamic problem, which is of the same form as that of Eqs (27) and (28) but with all functions involved being functions of space coordinates as well as of the frequency ω. This means that the final system of equations of the form of Eq. (31) has to be solved for a sequence of values of ω in order to produce the solution in the frequency domain as a function of ω in a discrete manner. If the external load is harmonic, then this frequency domain solution represents the amplitude of the solution and one has simply to multiply that solution by $e^{i\omega t}$ in order to obtain the time domain solution. If the external load is transient, this load is Fourier transformed, the problem is solved in the frequency domain and the time domain solution is finally obtained by a numerical inversion of the transformed solution. Both direct and inverse Fourier transforms are done numerically by the FFT algorithm (Polyzos et al 2005).

7 Numerical examples

In this section some representative numerical examples are presented in order to illustrate the BEM as applied to static and dynamic strain gradient elastic problems and demonstrate its advantages.

7.1 Example 1

Consider a 3D/2D problem dealing with the tension of a cylindrical / rectangular strain gradient elastic bar as shown in Fig. 1. This example has been taken from Karlis et al (2010). The height of the cylinder / rectangle is much smaller than its diameter / width (d = 4.2m, h = 1.2m). It is assumed that the Poisson's ratio ν = 0 and that there is only one gradient elastic constant in the model. Thus, one can compare numerical results across the axis of symmetry with one-dimensional (1D) analytical results (Tsepoura et al 2002).

The bar is subjected to a tension T_o = 2.1 GPa on its top and bottom sides, the modulus of elasticity E = 2.1 GPa and the gradient coefficient g takes the values 0.001, 0.05 and 0.1. The non-classical boundary condition applied at the top and bottom faces of the bar is$(q_x, q_y, q_z) = (0,0,0)$, while for all edges (in 3D) and corners (in 2D) the jump traction is$(E_x, E_y, E_z) = (0,0,0)$. The side surface of the bar is left traction free by imposing there $(P_x, P_y, P_z) = (0,0,0)and(R_x, R_y, R_z) = (0,0,0)$.

The 3D problem has been solved with octant symmetry, whereas in the 2D case of the rectangular bar only one quarter of the domain has been discretized. For the 2D case, approximately 50 elements have been used, whereas for the 3D case, up

to 150 elements have been utilized. A set of internal points has been placed along the central vertical axis of the bar. In Fig. 2, the axial displacements of the internal points are presented together with the 1D analytical results of Tsepoura et al (2002) having the form

$$w(z) = \frac{T_0}{E}\left[|z| - g\frac{\sinh\left(\frac{|z|}{g}\right)}{\cosh\left(\frac{|z|}{2g}\right)}\right], \quad |z| \leq \frac{h}{2} \tag{44}$$

For all the displayed results, the relative error with respect to the analytical solution is below 0.5%.

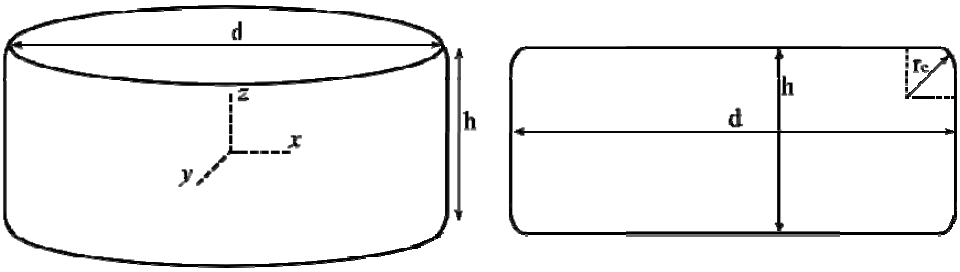

Figure 2: Geometry of the strain gradient elastic bar in three and two dimensions

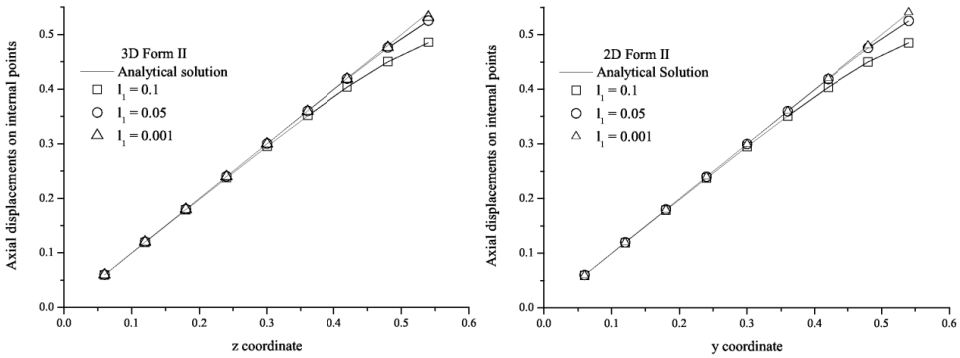

Figure 3: Axial displacements of internal points for (a) the 3D case and (b) the 2D case

8 Example 2

Consider a spherical cavity of radius α into an infinite strain gradient elastic 3D space subjected to a radially applied pressure P_0 and determine the resulting radial displacement. This problem has been taken form Tsepoura et al (2003).

The boundary conditions of the problem are

$$\mathrm{P}(a)=\mathrm{P}_0 \quad , \qquad \mathrm{R}(a)=\mathrm{P}_0 \tag{45}$$

and its analytical solution reads (Tsepoura et al 2003)

$$\mathrm{u}(\mathrm{r})=\mathrm{B}\frac{1}{\mathrm{r}^2}+\mathrm{D}\sqrt{\frac{\pi}{2(\mathrm{r/g})}}\mathrm{K}_{3/2}(\mathrm{r/g}) \tag{46}$$

$$\begin{aligned} B &= \frac{-P_0(1-2\nu)(1+\nu)a^3\left(6g^3+6g^2a+3ga^2+a^3\right)}{2E\left[3g^3(-3+4\nu)+3g^2(-3+4\nu)a+3g(-1+2\nu)a^2+(-1+2\nu)a^3\right]} \\ D &= -\frac{6e^{a/g}P_0(-1+2\nu)(1+\nu)\sqrt{g/r}a^4}{E\pi\sqrt{r/g}\left[3g^3(-3+4\nu)+3g^2(-3+4\nu)a+3g(-1+2\nu)a^2+(-1+2\nu)a^3\right]} \end{aligned} \tag{47}$$

with $\mathrm{K}_{3/2}$ being the modified Bessel function of the second kind and 3/2 order. Assuming α = 1, P_0/E = 1 and $\nu = 0$ one can use the BEM to determine the radial displacement u(r) and depict its variation with the distance r for various values of g as in Fig. 4. Due to the symmetry of the problem, only one octant of the sphere is discretized using 38 quadratic quadrilateral boundary elements. Figure 4 indicates an excellent agreement between the numerical results and those of the analytical solution.

8.1 Example 3

Consider a square strain gradient elastic plate of side $\mathrm{L}=16\alpha$ in a state of plane strain, as shown in Fig. 5. The plate contains a central horizontal line crack of length 2α and is subjected to a uniform tensile traction P_0 applied normal to its top and bottom sides. The corners of the plate are rounded with very small radii of curvature in order to have a smooth boundary. The applied traction P_0 = 100 MPa, the Young's modulus and Poisson's ratio of the strain gradient elastic plate are E = 210 GPa and $\nu = 0.2$, respectively, while the length $\alpha = 0.5m$. Due to the double symmetry of the problem, only one quarter of the plate is discretized, as shown in Fig. 5, with the following boundary conditions along the axes of symmetry:

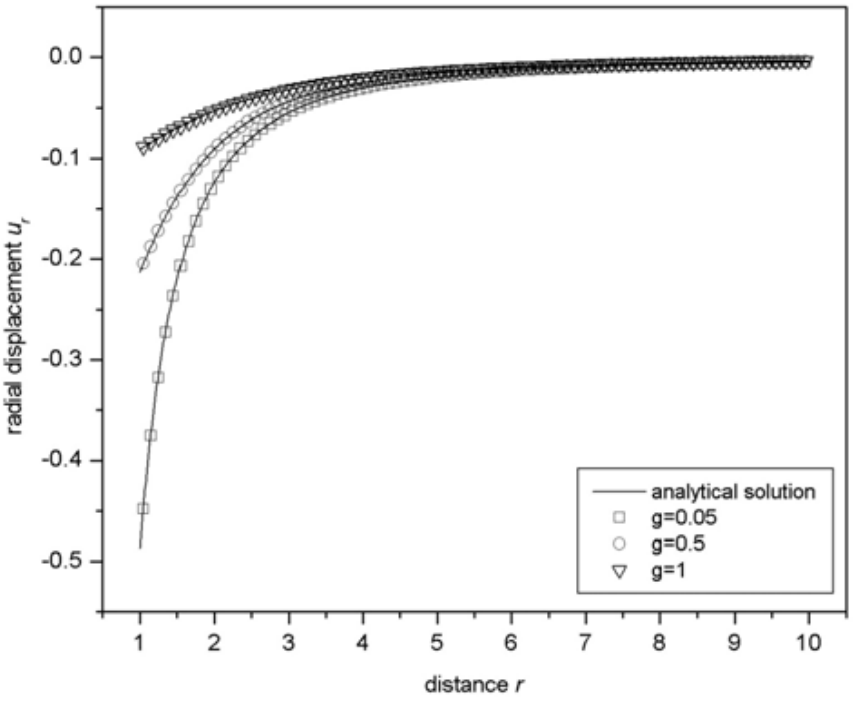

Figure 4: Radial displacement u_r versus radial distance of the spherical cavity of radius α, for various values of g

$\mathrm{P}(x,0)=0$ and $\mathrm{R}(x,0)=0$ for $0\le x<\alpha$, $u_y(x,0)=0$ and $\mathrm{R}(x,0)=0$ for $\alpha\le x\le L/2$ and $u_x(0,y)=0$ and $\mathrm{R}(0,y)=0$ for $0\le y\le L/2$.

This problem and its solution have been taken from Karlis et al (2007). Its solution, obtained by the BEM in conjunction with the use of the special crack tip element described in section 5, consists mainly of the crack opening displacement profile and the stress intensity factors (SIF's). Extensive convergence studies in Karlis et al (2007) have shown that a ratio of $\alpha/\ell_e=8$ leads to very good results, where α is the half length of the crack and ℓ_e the length of the special crack-tip boundary elements.

Figure 6 displays the upper-right-quarter of the crack opening displacement profile obtained by the present BEM for four different values of the gradient coefficient g (0.01, 0.1, 0.3, 0.5). In the same figure, the crack profile provided by the classical elasticity theory (g = 0) is also shown. The main conclusion here is that the crack profile of the gradient elastic case remains sharp at the crack tip and is not blunted as in the classical case. This cusp type of profile is identical to the one coming out

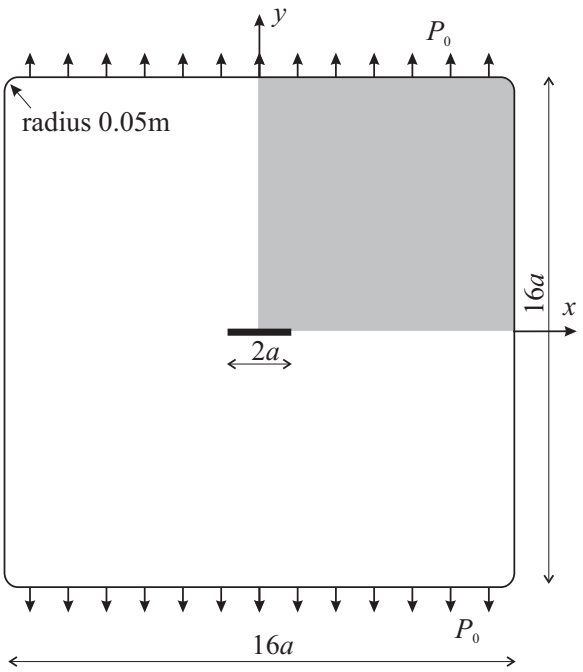

Figure 5: Strain gradient elastic plate with a central horizontal line crack

of Barenblatt's (1962) cohesive zone theory. Also, it should be noticed that as the gradient coefficient g increases, the crack becomes stiffer.

The two mode I SIFs for the gradient elastic case, $(K_I)_1$ and $(K_I)_2$, are plotted versus the gradient coefficient g in Fig. 7. The interesting remark here is that the SIF $(K_I)_1$ tends to zero as the gradient coefficient g tends to zero. As a result of that, Eq. (36) becomes $P_y = (K_I)_2/\sqrt{2\pi}\lim_{r\to 0} r^{-1/2}$ with $(K_I)_2$ being the mode I SIF as defined in classical elasticity theory. Furthermore, all SIFs decrease for increasing values of the gradient coefficient g. However, the most important observation here is that the SIF $(K_I)_1$ takes only negative values. This means that in gradient elasticity the stresses near the crack tip not only go to infinity with a different order $(r^{-3/2})$ than that of classical elasticity $(r^{-1/2})$, but are also compressive and not tensile as in classical elasticity. This explains the different shapes of the crack profile in gradient and classical elasticity theories, as shown in Fig. 6.

8.2 Example 4

Consider a spherical cavity of radius α into an infinite gradient elastic medium subjected to a radial pressure P of magnitude P_0 i) harmonically varying with time

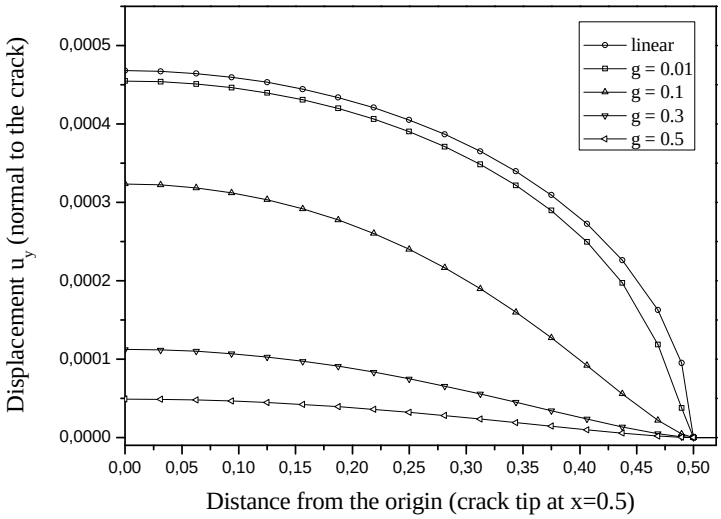

Figure 6: Shape of mode I crack for different values of the gradient coefficient g.

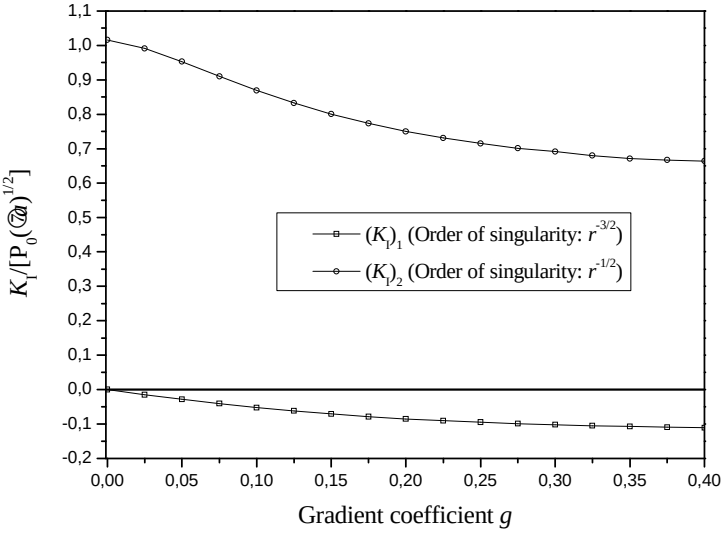

Figure 7: SIFs as functions of g for mode I crack

$\left(P = P_0 e^{i\omega t}\right)$ and ii) suddenly applied $(P = P_0 H(t-\tau)$ with $\tau = 3sec)$. In the above, ω represents frequency and H(t) stands for the Heaviside function. One is interested in the radial displacement $u(r,\ \omega)$ and $u(r,\ t)$ for the two above kinds of applied loading. This example has been taken from Polyzos et al (2005).

The boundary conditions of the problem are of the same form as Eqs. (45) of the corresponding static version of the problem. The problem associated with the harmonic time variation of the load can be easily solved analytically in the frequency domain and its solution has the form (Polyzos et al 2005)

$$u_r(r) = \frac{A_1}{A_2 a} h_1^{(1)}(k_1 r) + \frac{B_1}{B_2 a}\sqrt{\frac{\pi}{2(m_1 r)}}\mathrm{K}_{\frac{3}{2}}(m_1 r) \tag{48}$$

where

$$A_1 = -(k_1^2 P_0 a^3 (3gc_1(a^2 + g^2(2 + a^2 k_1^2)) + c_1^2 a(a^2 + g^2(6 + a^2 k_1^2)))) \tag{49}$$

$$B_1 = -((e^{\frac{c_1 a}{g}} g c_1^2 P_0 a^3 (-6i + k_1 a(-6 + k_1 a(3i + k_1 a)))) \tag{50}$$

$$\begin{aligned} B_2 = (\mu\ \pi(&-18ig^3 c_2 - 18g^2 c_2 c_3 a - 6igc_2 a^2 + 2c_3(-3 - 10c_3^2 - 6c_3^4)a^3 + \\ &3ic_3 k_1(1 + 3c_3^2 + 2c_3^4)a^4 + c_3^3 k_1^2 c_1^2 a^5 + \\ &c_1 a(-18ig^2 c_2 - 18gc_2 c_3 a - 2i(1 - 2c_3^2 - 6c_3^4)a^2 - 2k_1 c_2 a^3 + i(k_1 + k_1 c_3^2)^2 a^4)))) \end{aligned} \tag{51}$$

In the above, $m_1 = \sqrt{1 + g^2 k_1^2}/g$, $c_1 = \sqrt{1 + g^2 k_1^2}$, $c_2 = 1 + 2g^2 k_1^2$, $c_3 = gk_1$, $b_1 = 1 + 3c_3^2 + 2c_3^4$, $b_2 = 1 - 2c_3^2 - 6c_3^4$, $\mu = E/2(1+\nu)$, $i = \sqrt{-1}$ while $h_1^{(1)}(k_1 r)$ and $\sqrt{\pi/(2m_1 r)}K_{3/2}(m_1 r)$ are, the third order spherical Bessel function of the first kind and the first order modified Bessel function of the second kind, respectively.

Assuming $\alpha = 1$ and $P_0 = 1$ and discretizing only one octant of the spherical cavity (due to the symmetry), displacement amplitudes for different values of the gradient coefficient g and for the excitation frequencies $\omega = 0.002 rad/s$ and $\omega = 40 rad/s$, are evaluated by the BEM and depicted in Figs. 8 and 9, respectively, as functions of distance r form the centre of the spherical cavity. As it is evident from Figs. 8 and 9 the agreement between the BEM and the analytical solutions is excellent. It is also observed that, while for very small frequencies the solution almost coincides with the static one (Fig. 4), as expected, for higher frequencies there are oscillations with amplitude decreasing with distance.

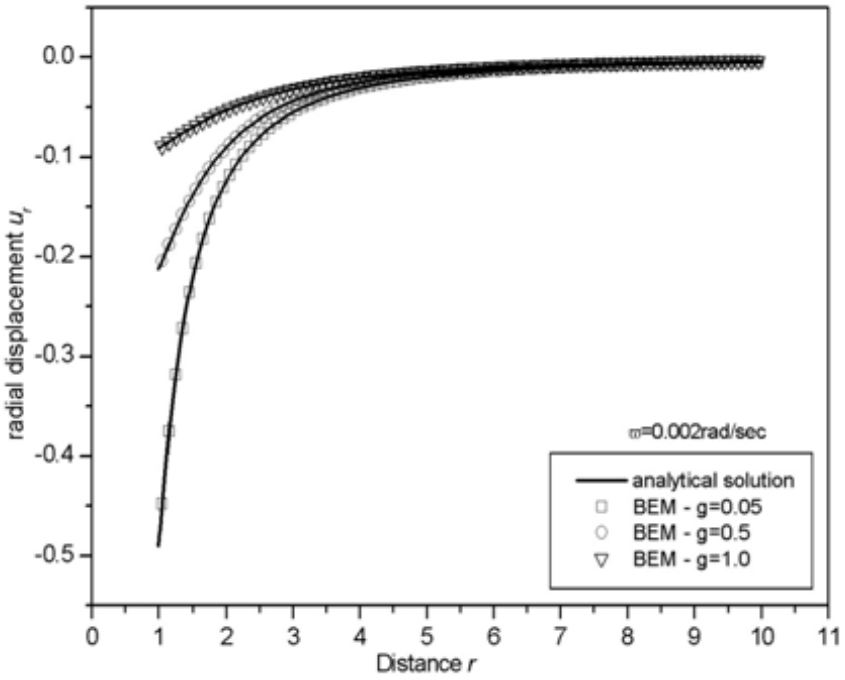

Figure 8: Displacement u_r versus distance r for various values of g and $\omega = 0.002 rad/s$

When the load is transient (suddenly applied) the problem is solved in the Fourier transform (frequency) domain and the time domain response is obtained by a numerical inversion of the transformed solution through the Fast Fourier Transform (FFT) algorithm. Figure 10 shows the axial displacement versus time at the point r = 1.05 for various values of g. The classical solution of the problem (for g = 0) taken from Timoshenko and Goodier (1970) is also depicted in Fig. 10 for reasons of comparison. From Fig. 10 one can observe that the response decreases for increasing values of g.

9 Conclusions and future developments

On the basis of the material presented in the preceding sections, the following conclusions and suggestions for future developments can be stated:

1. The fundamental solution, the reciprocity identity and the integral representation of the strain gradient elastic problem in the context of Mindlin's form

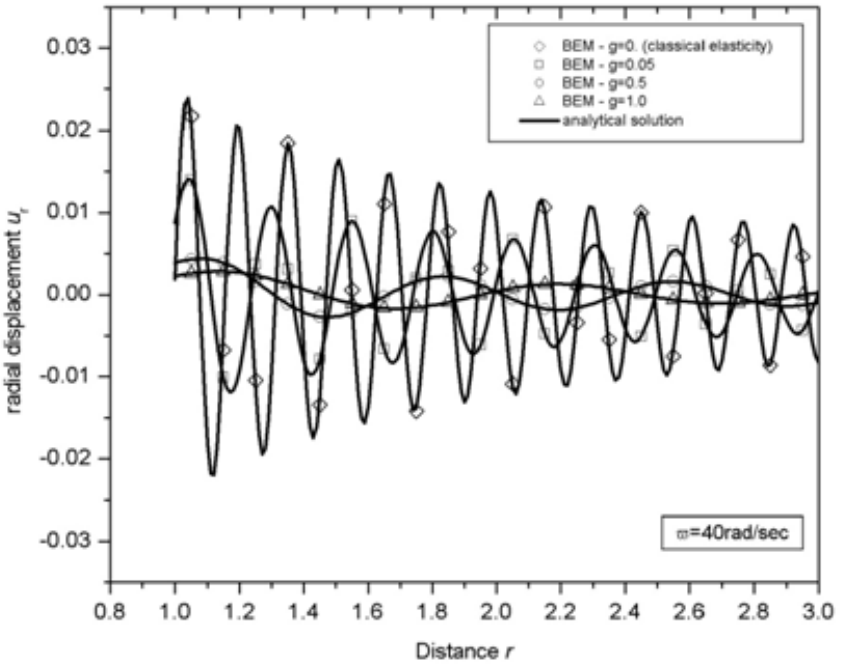

Figure 9: Displacement u_r versus distance r for various values of g and $\omega = 40 rad/s$

II strain gradient elastic theory and its simplifications have been developed.

2. An advanced and accurate boundary element method for solving two and three dimensional static and frequency domain dynamic strain gradient elastic problems has been proposed.

3. A special boundary element method for solving two and three dimensional strain gradient elastic fracture mechanics problems has also been developed. This works with special crack-tip (front) elements resulting in a direct determination of stress intensity factors via the nodal traction values of these elements.

4. The boundary element method is the ideal tool for solving strain gradient elastic problems of complex geometry and boundary conditions because, unlike the finite element method, i) reduces the dimensionality of the problem by one thereby restricting the discretization to the boundary of the domain, ii) provides highly accurate results, especially near high stress gradients, iii)

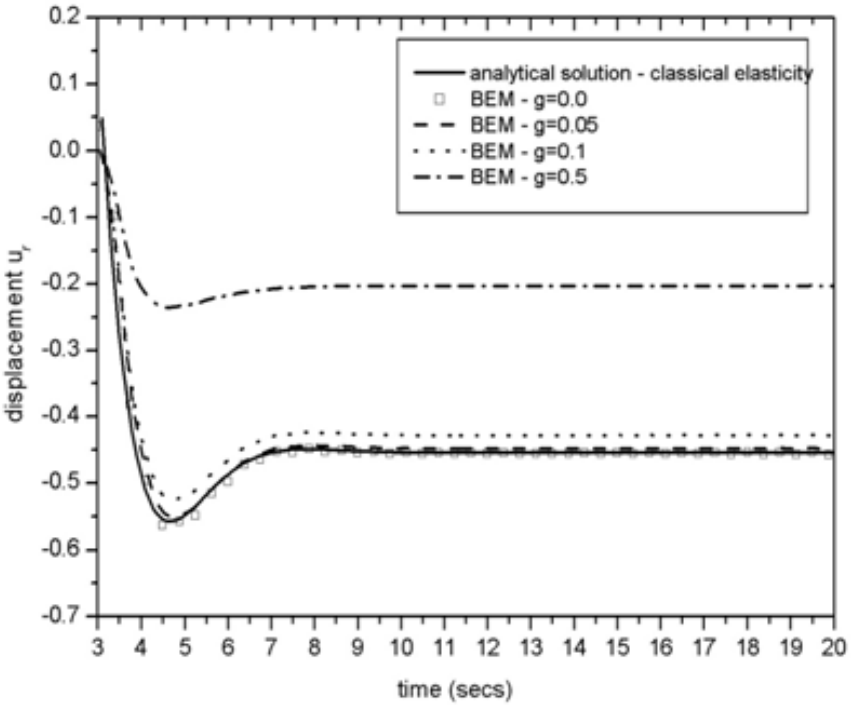

Figure 10: Displacement u_r versus time for various values of g

does not need absorbing boundaries for infinite or semi-infinite domains and iv) does not require any continuity requirements. Finally, the old efficiency problem due to the presence of non-symmetric matrices has been resolved with the use of highly efficient equation solvers.

5. Use of the boundary element method in strain gradient elastic problems under static or dynamic loading conditions can help one to easily assess the importance of microstructural effects, such as size effects, reduction or elimination of singularities, wave dispersion and appearance of a cohesion zone in cracks.

6. In spite of all the above advantages of the method, there are some limitations at its present stage of development, which should be taken care of in the near future. These are the numerical evaluation of internal and near to the boundary stresses as well as the proper treatment of non-smooth boundaries (corners and edges).

Acknowledgement: The authors would like to thank Mrs M. Dimitriadi for her excellent typing of the manuscript.

References

Akarapu, S.; Zbib, H.M. (2006): Numerical analysis of plane cracks in strain-gradient elastic materials, *Int. J. Fracture*, vol. 141, pp. 403-430.

Altan, B.S.; Aifantis, E.C. (1992): On the structure of the mode – III crack – tip in gradient elasticity, *Scripta Metall. Mater.*, vol. 26, pp. 319-324.

Altan, B.S.; Evensen, H.A.; Aifantis, E.C. (1996): Longitudinal vibrations of a beam: a gradient elasticity approach, *Mech. Res. Commun.*, vol. 23, pp. 35-40.

Amanatidou, E.; Aravas, N. (2002): Mixed finite element formulations of strain-gradient elasticity problems, *Comput. Methods Appl. Mech. Engng.*, vol. 191, pp. 1723-1751.

Aravas, N. (2011): Plane strain problems for a class of gradient elasticity models-A stress function approach, *J. Elasticity*, vol. 104, pp. 45-70.

Askes, H.; Aifantis, E.C. (2006): Gradient elasticity theories in statics and dynamics-a unification of approaches, *Int. J. Fracture,* vol. 139, pp. 297-304.

Askes, H.; Aifantis, E.C. (2011): Gradient elasticity in statics and dynamics: an overview of formulations, length scale identification procedures, finite element implementations and new-results, *Int. J. Solids Struct.*, vol. 48, pp. 1962-1990.

Askes, H.; Bennett, T.; Aifantis, E.C. (2007): A new formulation and C^0 – implementation of dynamically consistent gradient elasticity, *Int. J. Num. Meth. Eng.,* vol. 72, pp. 111-126.

Askes, H.; Gutierrez, M.A. (2006): Implicit gradient elasticity, *Int. J. Numer. Meth. Engng.*, vol. 67, pp. 400-416.

Askes, H.; Morata, I.; Aifantis, E.C. (2008): Finite element analysis with staggered gradient elasticity, *Comput. Struct.*, vol. 86, pp. 1266-1279.

Askes, H.; Wang, B.; Bennett, T. (2008): Element size and time step selection procedures for the numerical analysis of elasticity with higher-order inertia, *J. Sound Vibr.*, vol. 314, pp. 650-656.

Bennett, T.; Askes, H. (2009): Finite element modeling of wave dispersion with dynamically consistent gradient elasticity, *Comput. Mech.*, vol. 43, pp. 815-825.

Bennett, T.; Gitman, I.M.; Askes, H. (2007): elasticity theories with higher order gradients of inertia and stiffness for the modeling of wave dispersion in laminates, *Int. J. Fracture*, vol. 148, pp. 185-193.

Beskos, D.E. (1987): Boundary element methods in dynamic analysis, *Appl. Mech.*

Rev., ASME, vol. 40, pp. 1-23.

Beskos, D.E. (1997): Boundary element methods in dynamic analysis, Part II (1986-1996), *Appl. Mech. Rev. ASME*, vol. 50, pp. 149-197.

Beskos, D.E. (2003): *Dynamic analysis of structures and structural systems, in Boundary Element Advances in Solid Mechanics,* Beskos, D.E. and Maier, G., Editors, Springer-Verlag, Wien, pp. 1-50.

Chang, C.S.; Gao J. (1997): Wave propagation in granular rod using high-gradient theory, *J. Eng. Mech. ASCE*, vol. 123, pp. 52-59.

Cosserat, E.; Cosserat, F. (1909): *Theories des Corps Deformables*, Hermann et Fils, Paris.

Dessouky, S.; Masad, E.; Little, D.; Zbib, H. (2006): Finite-element analysis of hot mix asphalt microstructure using effective local material properties and strain gradient elasticity, *J. Eng. Mech., ASCE*, vol. 132, pp. 158-171.

Engel, G.; Garikipati, K.; Hughes, T.J.R.; Larson, M.G.; Mazzei, L.; Taylor, R.L. (2002): Continuous/discontinuous finite element approximations of fourth-order elliptic problems in structural and continuum mechanics with applications to thin beams and plates, and strain gradient elasticity, *Comput. Methods Appl. Mech. Eng.*, vol. 191, pp. 3669-3750.

Eringen, C.A. (1966): Linear theory of micropolar elasticity, *J. Math. Mech.*, vol. 15, pp. 909-923.

Exadactylos, G.E.; Vardoulakis, I. (2001): Microstructure in linear elasticity and scale effects: a reconsideration of basic rock mechanics and rock fracture mechanics, *Tectonophysics*, vol. 335, pp. 81-109.

Filopoulos, S.P.; Papathanasiou, T.K.; Markolefas, S.I.; Tsamasphyros, G.J. (2010): Dynamic finite element analysis of a gradient elastic bar with micro-inertia, *Comput. Mech.*, vol. 45, pp. 311-319.

Fischer, P.; Klassen, M.; Mergheim, J.; Steinmann, P.; Müller, R. (2011): Isogeometric analysis of 2D gradient elasticity, *Comput. Mech.,* vol. 47, pp. 325-334.

Fischer, P.; Mergheim, J.; Steinmann, P. (2010): On the C^1 continuous discretization of non-linear gradient elasticity: A comparison of NEM and FEM based on Bernstein-Bezier patches, *Int. J. Num. Meth. Eng.,* vol. 82, pp. 1282-1307.

Gao, X.L.; Ma, H.M. (2009): Green's function and Eshelby's tensor based on a simplified strain gradient elasticity theory, *Acta Mech.*, vol. 207, pp. 163-181.

Georgiadis, H.G.; Anagnostou, D.S. (2008): Problems of Flamant-Boussinesq and Kelvin type in dipolar gradient elasticity, *J. Elasticity*, vol. 90, pp. 71-98.

Georgiadis, H.G. (2003): The mode-III crack problem in microstructured solids

governed by dipolar gradient elasticity: static and dynamic analysis, *J. Appl. Mech., ASME*, vol. 70, pp. 517-530.

Georgiadis, H.G.; Vardoulakis, I.; Lykotrafitis, G. (2000): Torsional surface waves in a gradient-elastic half-space, *Wave Motion*, vol. 31, pp. 333-348.

Georgiadis, H.G.; Vardoulakis, I.; Velgaki, E.G. (2004): Dispersive Rayleigh-wave propagation in microstructured solids characterized by dipolar gradient elasticity, *J. Elasticity,* vol. 74, pp. 17-45.

Giannakopoulos, A.E.; Amanatidou, E.; Aravas, N. (2006): A reciprocity theorem in linear gradient elasticity and the corresponding Saint-Venant principle, *Int. J. Solids Struct.,* vol. 43, pp. 3875-3894.

Giannakopoulos, A.E.; Stamoulis, K. (2007): Structural analysis of gradient elastic components, *Int. J. Solids Struct.*, vol. 44, pp. 3440-3451.

Gitman, I.M.; Askes, H.; Kuhl, E.; Aifantis, E.C. (2010): Stress concentrations in fractured compact bone simulated with a special class of anisotropic gradient elasticity, *Int. J. Solids Struct.,* vol. 47, pp. 1099-1107.

Hadjesfandiari, A.R.; Dargush, G.F. (2012): Boundary element formulation for plane problems in couple stress elasticity, *Int. J. Num. Meth. Eng.*, vol. 89(5), pp. 618-636.

Imatani, S.; Hataday, K.; Maugin, G.A. (2005): Finite element analysis of crack problems for strain gradient material model, *Philos. Magazine,* vol. 85, pp. 4245-4256.

Karlis, G.F.; Charalambopoulos, A.; Polyzos, D. (2010): An advanced boundary element method for solving 2D and 3D static problems in Mindlin's strain-gradient theory of elasticity, *Int. J. Num. Meth. Eng.*, vol. 83, pp. 1407-1427.

Karlis, G.F.; Polyzos, D.; Tsinopoulos, S.V.; Vavva, M.G.; Fotiadis, D.I. (2007): *A BEM study on the wave propagation of guided waves in plates with microstructural effects*, in Advanced Topics in Scattering and Biomedical Engineering, A. Charalambopoulos, D.I. Fotiadis and D. Polyzos, Editors, World Scientific, Singapore, pp. 162-170.

Karlis, G.F.; Tsinopoulos, S.V.; Polyzos, D.; Beskos, D.E. (2007): Boundary element analysis of mode I and mixed mode (I and II) crack problems of 2-D gradient elasticity, *Comput. Methods Appl. Mech. Engng.,* vol. 196, pp. 50925103.

Karlis, G.F.; Tsinopoulos, S.V.; Polyzos, D.; Beskos, D.E. (2008): 2D and 3D boundary element analysis of mode-I cracks in gradient elasticity, *CMES: Computer Modeling in Engineering & Sciences*, vol. 26, pp. 189-207.

Koiter, W.T. (1964): Couple stresses in the theory of elasticity, I & II, Proc. Royal Netherlands Acad. Sci. (K. Ned. Akad. Wet.) B, vol. 67, pp. 17-44.

Lam, D.C.C. ; Yang, F.; Chong, A.C.M.; Wang, J.; Tong, P. (2003): Experiments and theory in strain gradient elasticity, *J. Mech. Phys. Solids*, vol. 51, pp. 1477-1508.

Lazar,M.; Maugin,G.A. (2005): Nonsingular stress and strain fields of dislocations and disclinations in first strain gradient elasticity, *Int. J. Eng. Sci.*, vol. 43, pp. 1157-1184.

Liu, Y.J. (2009): *Fast Multipole Boundary Element Method: Theory and Applications in Engineering*, Cambridge University Press, Cambridge, U.K.

Markolefas, S.I.; Tsouvalas, D.A.; Tsamasfyros, G.I. (2009): Mixed finite element formulation for the general anti-plane shear problem, including mode III crack computations, in the framework of dipolar linear gradient elasticity, *Comput. Mech.*, vol. 43, pp. 715-730.

Markolefas, S.I.; Tsouvalas, D.A.; Tsamasphyros, G.I. (2007): Theoretical analysis of a class of mixed, C^0 continuity formulations for general dipolar gradient elasticity boundary value problems, *Int. J. Solids Struct.*, vol. 44, pp. 546-572.

Markolefas, S.I.; Tsouvalas, D.A.; Tsamasphyros, G.I. (2008): Some C^o – continuous mixed formulations for general dipolar linear gradient elasticity boundary value problems and the associated energy theorems, *Int. J. Solids Struct.*, vol. 45, pp. 3255-3281.

Mindlin, R.D. (1964): Micro-structure in linear elasticity, *Arch. Rat. Mech. Anal.*, vol. 16, pp. 51-78.

Papacharalampopoulos, A.; Karlis, G.; Charalambopoulos, A.; Polyzos, D. (2010): An advanced boundary element method for solving 2D and 3D dynamic problems in Mindlin's gradient theory of elasticity, *CMES: Computer Methods in Engineering & Science*, Vol.58(1), pp.45-74.

Papacharalampopoulos, A.; Vavva, M.G.; Protopappas, V.C.; Fotiadis, D.I.; Polyzos, D. (2011): A numerical study on the propagation of Rayleigh and guided waves in cortical bone according to Mindlin's Form II gradient elastic theory, *Journal of Acoustical Society of America*, 130(2), pp.1060-1070.

Papanicolopulos, S.A.; Zervos, A. (2010): Numerical solution of crack problems in gradient elasticity, *Engng. Comput. Mech., ICE*, vol. 163, pp. 73-82.

Papanicolopulos, S.A.; Zervos, A.; Vardoulakis, I. (2009): A three-dimensional C^1 finite element for gradient elasticity, *Int. J. Num. Meth. Eng.*, vol. 77, pp. 1396-1415.

Papargyri-Beskou, S.; Beskos, D.E. (2008): Static, stability and dynamic analysis of gradient elastic flexural Kirchhoff plates, *Arch. Appl. Mech.*, vol. 78, pp. 625-635.

Papargyri-Beskou, S.; Beskos, D.E. (2008): Static, stability and dynamic analysis of gradient elastic flexural Kirchhoff plates, *Arch. Appl. Mech.,* vol. 78, pp. 625-635.

Papargyri-Beskou, S.; Beskos, D.E. (2009): Stability analysis of gradient elastic circular cylindrical shells, *Int. J. Eng. Sci.*, vol. 47, pp. 1379-1385.

Papargyri-Beskou, S.; Giannakopoulos, A.E.; Beskos, D.E. (2010): Variational analysis of gradient elastic flexural plates under static loading, *Int. J. Solids Struct.*, vol. 47, pp. 2755-2766.

Papargyri-Beskou, S.; Polyzos, D.; Beskos, D.E. (2003): Dynamic analysis of gradient elastic flexural beams, *Struct. Eng. Mech.*, vol. 15, pp. 705-716.

Papargyri-Beskou, S.; Polyzos, D.; Beskos, D.E. (2009): Wave dispersion in gradient elastic solids and structures: A unified treatment, *Int. J. Solids Struct.,* vol. 46, pp. 3751-3759.

Papargyri-Beskou, S.; Tsepoura, K.G.; Polyzos, D.; Beskos, D.E. (2003): Bending and stability analysis of gradient elastic beams, *Int. J. Solids Struct.*, vol. 40, pp. 385-400.

Polyzos, D. (2005): 3D Frequency domain BEM for solving dipolar gradient elastic problems, *Comput. Mech.*, vol. 35, pp. 292-304.

Polyzos, D.; Fotiadis, D.I. (2012): Derivation of Mindlin's gradient elastic theory via simple lattice and continuum models, *International Journal of Solids and Structures,* 49, pp. 470–480, 2012.

Polyzos, D.; Tsepoura, K.G.; Beskos, D.E. (2003): BEM solutions of frequency domain gradient elastodynamic 3-D problems, *Electr. J. Bound. Elem.,* vol. 1, pp. 174-200.

Polyzos, D.; Tsepoura, K.G.; Beskos, D.E. (2005): Transient dynamic analysis of 3-D gradient elastic solids by BEM, *Comput. Struct.*, vol. 83, pp. 783-792.

Polyzos, D.; Tsepoura, K.G.; Tsinopoulos, S.V.; Beskos, D.E. (2003): A boundary element method for solving 2-D and 3-D static gradient elastic problems. Part I: Integral formulation, *Comput. Meth. Appl. Mech. Eng.,* vol. 192, pp.2845-2873.

Ru, C.Q.; Aifantis, E.C. (1993): A simple approach to solve boundary – value problems in gradient elasticity, *Acta Mech.*, vol. 101, pp. 59-68.

Shu, J.Y.; King, W.E.; Fleck, N.A. (1999): Finite elements for materials with strain gradient effects, *Int. J. Numer. Meth. Engng.,* vol. 44, pp. 373-391.

Soh, A.K.; Chen, W.J. (2004): Finite element formulations of strain gradient theory for microstructures and the C0-1 patch test, *Int. J. Num. Meth. Eng.*, vol. 61, pp. 433-454.

Tang, Z.; Shen, S.; Atluri, S.N. (2003): Analysis of materials with strain-gradient effects: A meshless local Petrov-Galerkin (MLPG) approach with nodal displacements only, *CMES: Computer Modeling in Engineering & Sciences*, vol. 4, pp. 177-196.

Tenek, L.T.; Aifantis, E.C. (2002): A two-dimensional finite element implementation of a special form of gradient elasticity, *CMES: Computer Modeling in Engineering & Sciences*, vol. 3, pp. 731-741.

Tiersten, H.F.; Bleustein, J.L. (1974): *General elastic continua,* pp. 67-metricconverterProductID1 in103, in Hermann, G. (Editor.), R.D. Mindlin and Applied Mechanics, Pergamon Press, New York.

Toupin, R.A. (1962): Elastic materials with couple-stresses, *Arch. Rat. Mech. Anal.*, vol. 11, pp. 385-414.

Tsamasphyros, G.I.; Markolefas, S.; Tsouvalas, D.A. (2007): Convergence and performance of the h- and p- extensions with mixed finite element C^0 – continuity formulations, for tension and buckling of a gradient elastic beam, *Int. J. Solids Struct.*, vol. 44, pp. 5056-5074.

Tsamasphyros, G.I.; Vrettos, C.D. (2010): A mixed finite volume formulation for the solution of gradient elasticity problems, *Arch. Appl. Mech.,* vol. 80, pp. 609-627.

Tsepoura, K.G.; Papargyri-Beskou, S.; Polyzos, D. (2002): A boundary element method for solving 3-D static gradient elastic problems with surface energy, *Comput. Mech.,* vol. 29, pp. 361-381.

Tsepoura, K.G.; Papargyri-Beskou, S.; Polyzos, D.; Beskos, D.E. (2002): Static and dynamic analysis of gradient elastic bars in tension, *Arch. Appl. Mech.*, vol. 72, pp. 483-497.

Tsepoura, K.G.; Polyzos, D. (2003): Static and harmonic BEM solutions of gradient elasticity problems with axisymmetry, *Comp. Mech.,* vol. 32, pp. 89-103.

Tsepoura, K.G.; Polyzos, D. (2003): Static and harmonic BEM solutions of gradient elasticity problems with axisymmetry, *Comput. Mech.,* vol. 32, pp. 89-103.

Tsepoura, K.G.; Tsinopoulos, S.; Polyzos, D.; Beskos, D.E. (2003): A boundary element method for solving 2-D and 3-D static gradient elastic problems. Part II: Numerical implementation, *Comput. Meth. Appl. Mech. Eng., vol.* 192, pp. 2875-2907.

Tsiatas, G.C. (2009): A new Kirchhoff plate model based on a modified couple stress theory, *Int. J. Solids Struct.,* vol. 46, pp. 2757-2764.

Tsiatas, G.C. and Katsikadelis, J.T. (2011): A new microstructure-dependent Saint-Venant torsion model based on a modified couple stress theory, *Europ. J.*

Mech. A/Solids, vol. 30, pp. 741-747.

Vardoulakis, I.; Exadactylos, G.; Kourkoulis, S.K. (1998): Bending of marble with intrinsic length scales: a gradient theory with surface energy and size effects, *J. Phys. IV,* vol. 8, pp. 399-406.

Vardoulakis, I.; Sulem, J. (1995): *Bifurcation Analysis in Geomechanics,* Chapman and Hall, London.

Vavva, M.G.; Protopappas, V.C.; Gergidis, L. N.; Charalampopoulos, A.; Fotiadis, D. I.; Polyzos, D. (2009): Velocity dispersion curves of guided waves propagating in a free gradient elastic plate: application to cortical bone, *The Journal of Acoustical Society of America*, Vol. 125(5), pp. 3414–3427.

Vavva, M.G.; Protopappas, V.C.; Gergidis, L.N.; Charalambopoulos, A.; Fotiadis, D.I.; Polyzos, D. (2009): Velocity dispersion of guided waves propagating in a free gradient elastic plate: application to cortical bone, *J. Acoust. Soc. Amer.*, vol. 125, pp. 3414-3427.

Zervos, A. (2008): Finite elements for elasticity with microstructure and gradient elasticity, *Int. J. Num. Meth. Eng.*, vol. 73, pp. 564-595.

Zervos, A.; Papanicolopulos, S.A.; Vardoulakis, I. (2009): Two finite-element discretizations for gradient elasticity, *J. Eng. Mech. ASCE,* vol. 135, pp. 203-213.

Zhao. J.; Chen, W.J.; Lo, S.H. (2011): A refined nonconforming quadrilateral element for couple stress / strain gradient elasticity, *Int. J. Num. Meth. Eng.*, vol. 85, pp. 269-288.